A modified electrode by a facile green Preparation of reduced graphene oxide utiliz–ing olive leaves extract.

Article *in* Carbon letters · July 2017

DOI: 10.5714/CL.2017.24.047

CITATIONS
2

READS
111

3 authors, including:

Abeer Baioun
Damascus University
3 PUBLICATIONS **3** CITATIONS

SEE PROFILE

CARBON letters

Note

Carbon Letters Vol. 22, 110-114 (2017)

Li-ion battery anodes from ginkgo leaf-derived nanoporous carbons rich in redox-active heteroatoms

Na Rae Kim[1,*], Hong Joo An[1,*], Young Soo Yun[2,♠] and Hyoung-Joon Jin[1,♠]

[1]Department of Polymer Science and Engineering, Inha University, Incheon 22212, Korea
[2]Department of Chemical Engineering, Kangwon National University, Samcheok 25913, Korea

Article Info

Received 9 September 2016
Accepted 13 February 2017

♠Corresponding Author
E-mail: ysyun@kangwon.ac.kr
E-mail: hjjin@inha.ac.kr
Tel: +82-32-860-7483
*The authors have contributed equally in discussions of the work, performing the experiments, and writing the paper.

Open Access

DOI: http://dx.doi.org/10.5714/CL.2017.22.110

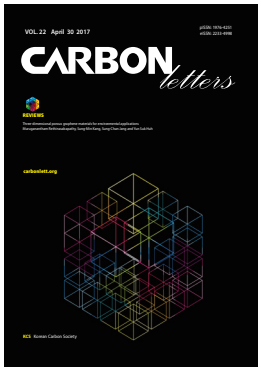

http://carbonlett.org

pISSN: 1976-4251
eISSN: 2233-4998

Lithium-ion batteries (LIBs) have attracted increasing attention as a sustainable power source due to the rapid growth in mobile electronics and electric automobile markets, driven by increasing environmental awareness [1-4]. The electrochemical performance of LIBs is strongly dependent on the active electrode materials. Therefore, their continuing advanced development is of key importance to meet the expectations of the market [5-7]. Graphite, commonly used in LIB anodes, forms binary graphite intercalation compounds with the formula LiC_6, via the intercalation of lithium ions at 0.1 V vs. Li^+/Li, corresponding to a capacity of ~372 mAh g^{-1} [8,9]. The favorable energy density and reversible charge/discharge cycles of graphite have contributed to the commercial success of conventional LIBs. Nevertheless, the new demands of state-of-the art applications require better energy and power characteristics, requiring the development of alternative anode materials that can surpass the electrochemical performance of graphite.

Nanoporous carbons (NPCs) have been utilized as LIB anodes due to their good kinetic properties and excellent energy storage characteristics [10,11]. NPCs provide efficacious Li-ion diffusion pathways because they contain extensive percolation networks, which originate from interconnected nanopores [12]. In addition, NPCs possess numerous active sites for Li-ion storage, including topological defects, edge defects, and heteroatoms [13,14]. NPCs fabricated from bio-waste provide additional advantages of sustainability, low cost, and simplicity of fabrication [15,16]. Fallen leaves, particularly ginkgo leaves, are considered to be good precursors for NPCs, because they are mainly composed of cellulose, which is known to be a good carbon source. Ginkgo leaves are also estimated to be one of the most abundant and ubiquitous tree waste products in nature [17]. The use of NPCs as a LIB anode material has been extensively reported [18-21]. Sun et al. [18] reported NPCs derived from spongy pomelo peels, showing a reversible capacity of ~452 mAh g^{-1}. Carbonaceous materials derived from green tea leaves have exhibited a specific capacity of 471 mAh g^{-1} [19]. Zhang et al. [20] reported NPCs fabricated from pine cones, with a specific capacity of 394 mAh g^{-1} and a coulombic efficiency of 99.0%. Hierarchical porous carbon obtained from fish scales showed a reversible capacity of 541.8 mAh g^{-1} and stable cycling performance (~75 cycles) [21]. These materials show improved capacities and rate performance compared to the conventional graphite anode. However, the above performances are highly variable, depending on the carbon precursors and the fabrication processes used. These results imply that better-performing NPCs could be prepared using optimized carbon precursors and synthetic methods. Therefore, more studies on the preparation of competitive NPCs from bio-waste are still required for high-performance LIBs.

In this study, nanoporous carbonaceous materials rich in heteroatoms (GL-NPCs) were fabricated from ginkgo leaves by simple carbonization/activation with potassium hydroxide followed by acid treatment. The GL-NPCs exhibited a high specific surface area of 1296 m^2 g^{-1} and a high heteroatom content (C/O and C/N atom ratios of 7.9 and 30.6, respectively). These properties led to superior electrochemical performance, featuring a high specific capacity of ~576 mAh g^{-1}, good rate capabilities at current densities from 0.1 to 2 A g^{-1}, and stable cycling.

Ginkgo leaves were collected from roadside trees near Inha University and successively washed several times with distilled water and ethanol (94.0%; OCI Co., Korea) to remove

surface-adsorbed impurities. After drying at 80°C, the dried leaves (5 g) were ground with KOH (10 g, 95%; Samchun Pure Chemical Co., Ltd., Korea) for 30 min using a mortar and pestle. The mixture was heated at 800°C under N_2 atmosphere in a tubular furnace at a heating rate of 10°C min^{-1}. The product was successively washed with distilled water and ethanol several times and then dried at 80°C. The resulting material was treated with 30 wt% nitric acid (60%; Daejung Chemicals & Metals Co., Ltd., Korea) at 60°C for 2 h under mild stirring. Finally, the as-prepared GL-NPCs were successively washed several times with water and ethanol and stored in a vacuum oven at 30°C.

The electrochemical characteristics of GL-NPCs were measured using a automatic battery cycler (Wonatech, Korea). For the half-cell tests, a CR2032-type coin cell was assembled in a glove box filled with argon gas using the sample as a working electrode and lithium foil as both the counter and reference electrodes. For the Li-ion cell, a 1 M $LiPF_6$ (99.99%; Aldrich, USA) solution in ethylene carbonate/dimethyl carbonate (EC/DMC) (1:1 v/v) was used as an electrolyte, and a glass microfiber filter (GF/F; Whatman, UK) was used as a separator. The working electrode was prepared by mixing the active material (70 wt%), super P as a conductive carbon (20 wt%), and polyvinylidene fluoride (10 wt%, average Mw ~534,000 by GPC, powder; Sigma-Aldrich) as a binder in N-methyl-2-pyrrolidone (99.7%; Daejung Chemicals & Metals Co., Ltd.). The slurries were coated on Cu foil (20 μm thickness) and dried in an oven at 80°C. The galvanostatic discharge/charge tests were carried out between 0.01 and 3.0 V at various current densities.

The morphologies of the GL-NPCs were characterized using field emission transmission electron microscopy (FE-TEM; JEM2100F, JEOL, Japan) and field emission scanning electron microscopy (S-4300; Hitachi, Japan). To investigate the microstructure of GL-NPCs, X-ray diffraction (XRD; Rigaku DMAX 2500) and Raman spectroscopy were employed. XRD analysis was performed using Cu K_α radiation (λ=0.154 nm) at 40 kV and 100 mA. Raman spectra were recorded using a continuous-wave linearly polarized laser (514 nm, 2.41 eV, 16 mW). The laser beam was focused using a 100× objective lens, resulting in a spot ~1 μm in diameter. The specific surface area and pore structure of the GL-NPCs were obtained from nitrogen adsorption/desorption isotherms recorded by a surface area, and porosimetry analyzer (ASAP 2020; Micromeritics, USA) at –196°C. In addition, their surface chemical properties were investigated using X-ray photoelectron spectroscopy (XPS; PHI 5700 ESCA, USA) with monochromatic Al K_α radiation (hν=1486.6 eV).

As shown in Fig. 1a and c, GL-NPCs are composed of micrometer-scale particles with irregular shape; a number of macropores were also observed with TEM and scanning electron microscopy imaging. High-resolution FE-TEM imaging shows an amorphous carbon structure without any long-range carbon ordering (Fig. 1b). The XRD pattern of the GL-NPCs features two broad peaks of the (002) and (100) planes of graphite centered at 23 and 44°, respectively (Fig. 1d). The above pattern indicated the amorphous carbon structure of the samples.

In contrast, the Raman spectrum of the GL-NPCs exhibited distinct *D* and *G* bands at ~1350 and ~1580 cm^{-1}, respectively (Fig. 1e). The *D* and *G* bands correspond to the disorder in the A_{1g} breathing mode of the six-fold aromatic ring close to the basal structure, and the hexagonal structure related to the E_{2g}

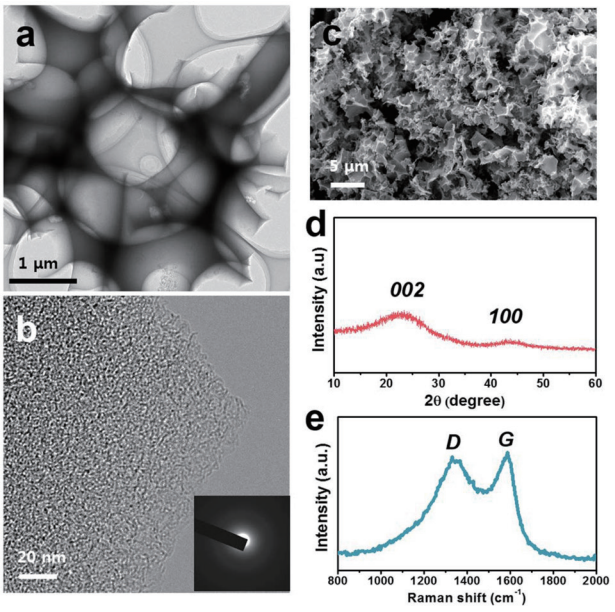

Fig. 1. The morphology and structural properties of nanoporous carbonaceous materials rich in heteroatoms (GL-NPCs). (a, b) Field emission transmission electron microscopy images of GL-NPCs. The inset image in (b) is the diffraction pattern of the samples. (c) Field emission scanning electron microscopy image of GL-NPCs. (d) X-ray diffraction pattern and (e) Raman spectrum of GL-NPCs.

vibration mode of the sp^2-hybridized C atoms, respectively. The in-plane crystal size of the hexagonal carbon structure (L_a) is approximately several nanometers, as determined by the intensity ratio of the *D* and *G* bands. These amorphous carbon structures could be the result of the KOH activation and carbonization.

The previously reported carbon activation mechanism by KOH can be divided into two steps, depending on the temperature [22]. Below 700°C, the consumption of carbon by oxygen is catalyzed by potassium metal, producing carbon monoxide and carbon dioxide. Following the above activation, metallic potassium ions are formed above 700°C. The formed metallic potassium penetrates the graphitic layers and expands the graphite lattice by rapidly removing the intercalated potassium. As a result, a highly defect-rich and porous carbon structure is produced.

The pore structure of the GL-NPCs was investigated using nitrogen adsorption and desorption isotherm tests (Fig. 2). The isotherm curves exhibited the International Union of Pure and Applied Chemistry type-I and type-IV hybrid shapes, suggesting a dual micro- and mesoporous structure (Fig. 2a). The adsorption of nitrogen gas at low relative pressure (P/P_0<0.01) is attributed to monolayer adsorption, which accounts for half of the adsorbed amount. The quantity of adsorbed nitrogen gradually increases until P/P_0~0.5, indicating that the GL-NPCs possess nanometer-scale pores.

In addition, hysteresis was observed in the adsorption and desorption curves of the GL-NPCs, allowing an estimation of the mesopore structure from its shape. The isotherm curves of the GL-NPCs exhibited an H4-type hysteresis loop, indicating the presence of narrow silt-like pores. The pore size distribution

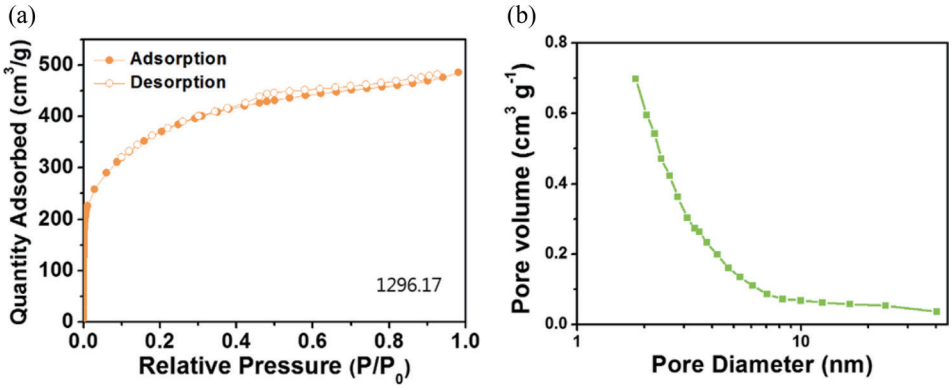

Fig. 2. (a) Nitrogen adsorption-desorption isotherms and (b) pore size distribution of the nanoporous carbonaceous materials rich in heteroatoms (GL-NPCs).

of the GL-NPCs is depicted in Fig. 2b, being relatively broad and composed of nanometer-scale pores of <10 nm. The large number of nanopores resulted in a high specific surface area of ~1296 m^2 g^{-1}.

The surface properties of the GL-NPCs were characterized by XPS (Fig. 3). Several distinct peaks were observed in the C 1s spectrum, centered at ~284.3 eV (C=C bonds), ~285.7 eV (C–O, C–N bonds), and ~289.8 eV (O–C=O bonds) (Fig. 3a). The O 1*s* spectrum shows two distinct peaks centered at ~532.8 eV and ~531.4 eV, attributed to C=O and C–O bonds, respectively (Fig. 3b). The nitrogen atoms existed in pyridine, pyridone/pyrrole, and N-oxide forms, as shown in Fig. 3c [23]. The C/O and C/N atom ratios were equal to 7.87 and 30.6, respectively, implying numerous heteroatoms doped on the GL-NPC surface. These heteroatoms can act as redox centers for Li-ion storage, improving the specific capacity.

The electrochemical properties of GL-NPCs as a LIB anode were investigated using a half-cell configuration, with 1 M $LiPF_6$ dissolved in EC/DMC (1:1 v/v) as an electrolyte, in a potential window of 0.01–3.0 V vs. Li^+/Li (Fig. 4). The galvanostatic discharge/charge profiles of the first three cycles at a current density of 100 mA g^{-1} are shown in Fig. 4a. For the first discharge curve, a change in voltage slope was observed between 1.0 and 0.5 V. This result agrees with the cyclic voltammogram shown in Fig. 4b. Therein, the first cathodic peak clearly appeared in the potential window of 1.0–0.5 V.

However, this peak was not observed in subsequent cycles, since it originates with the formation of an irreversible solid electrolyte interphase layer, which prevents further electrolyte decomposition after the first cycle [24]. The galvanostatic discharge/charge profiles show linear discharge/charge curves without plateaus (Fig. 4a). This is attributed to the absence of equivalent Li-ion storage sites, since GL-NPCs feature a disordered hexagonal carbon structure.

The reversible capacity of the GL-NPCs at a current density of 100 mA g^{-1} is ~576 mAh g^{-1}, which is much larger than that of graphite (~372 mAh g^{-1}). To investigate the contributions of capacitive and diffusion-controlled reactions to Li-ion storage, we analyzed the cyclic voltammetry (CV) curves at various scan rates (0.1 to 50 mV s^{-1}) using the following power-law relationship:

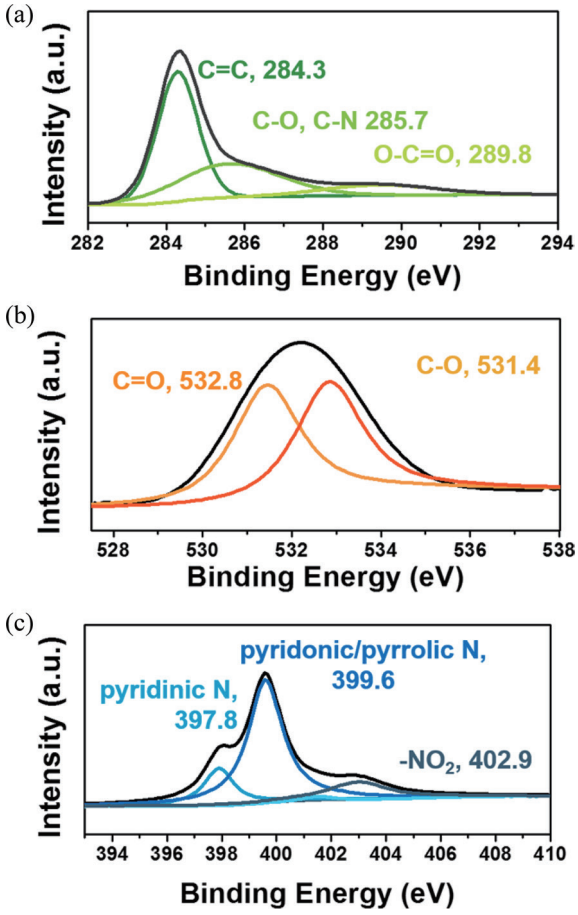

Fig. 3. (a) C 1s, (b) O 1s, and (c) N 1s X-ray photoelectron spectroscopy spectra of nanoporous carbonaceous materials rich in heteroatoms (GL-NPCs).

$$i = a v^b \quad (1)$$

, where i is the current (A), v is the scan rate (mV s^{-1}), and a and b are constants. For diffusion-controlled charge storage, the b-value is close to 0.5. In contrast, the b-value for surface-

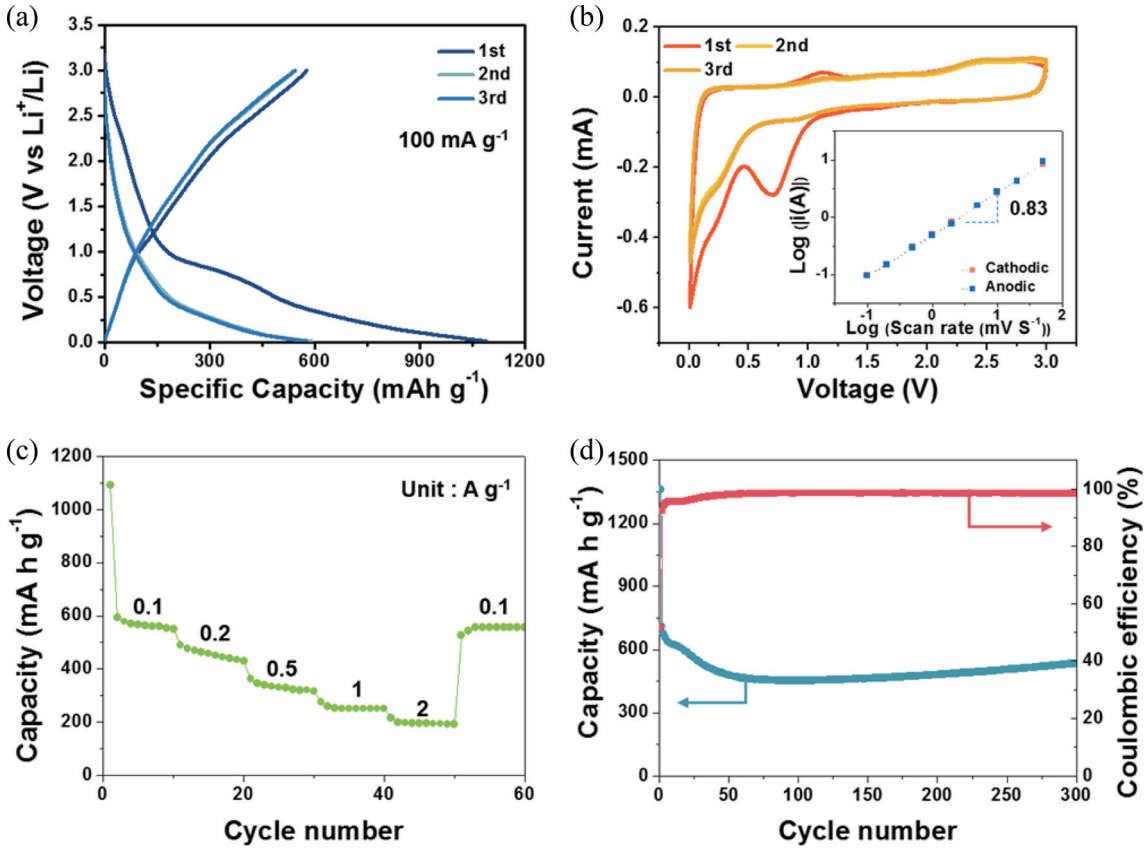

Fig. 4. Electrochemical properties of the nanoporous carbonaceous materials rich in heteroatoms (GL-NPCs) in a voltage window of 0.01 to 3.0 V vs. Li^+/Li in 1 M $LiPF_6$ dissolved in ethylene carbonate/dimethyl carbonate (EC/DMC) (1:1 v/v). (a) Galvanostatic discharge/charge profiles at 100 mA g^{-1}. (b) Cyclic voltammograms at a scan rate 0.1 mV s^{-1}. Inset is the *b*-value determination for the cathodic and anodic peak currents. (c) Rate performance of GL-NPCs at different current densities (0.1 to 2 A g^{-1}). (d) Cycling performance of GL-NPCs over 300 cycles at a current density of 0.5 A g^{-1}.

controlled charge storage is close to unity. The inset of Fig. 4b shows that the b-value of GL-NPCs is ~0.83, indicating that both diffusion-controlled and surface-controlled charge storage was involved [25,26].

Moreover, the GL-NPCs exhibited good rate performance (Fig. 4c), delivering reversible capacities of 560, 451, 328, 250, and 194 mAh g^{-1} at current densities of 0.1, 0.2, 0.5, 1, and 2 A g^{-1}, respectively. When the current density returned to 0.1 A g^{-1} after 50 cycles, the initial reversible capacity of GL-NPCs was restored, evidencing good kinetic performance. Fig. 4d demonstrates the cycling performance and coulombic efficiency of the GL-NPCs at a current density of 500 mA g^{-1}. A Coulombic efficiency of nearly 100% was observed, except for the initial few cycles. After the 100th cycle, the capacity steadily increased with cycle number, because the electrochemical active surface area was gradually increased. This phenomenon is also observed in a previously reported result based on reduced graphene oxide [27]. Moreover, GL-NPCs showed a high reversible capacity of ~533 mA h g^{-1} after 300 cycles.

GL-NPCs were fabricated from fallen ginkgo leaves by simple heating with KOH followed by acid treatment. This material had a high specific surface area of 1296 m^2 g^{-1}, showing a large number of nanopores and numerous heteroatoms (C/O and C/N atom ratios of 7.87 and 30.6, respectively). Due to their unique properties, GL-NPCs exhibited good electrochemical performances as a LIB anode. A high reversible capacity of 576 mA h g^{-1} was achieved at a current density of 100 mA g^{-1}, and a specific capacity of ~194 mAh g^{-1} was maintained at a 20-fold increased current rate. In addition, GL-NPCs showed stable cycling performance over 300 cycles.

Conflict of Interest

No potential conflict of interest relevant to this article was reported.

Acknowledgements

This work was supported by Inha University Research Grant (2017).

References

[1] Tarascon JM, Armand M. Issues and challenges facing rechargeable lithium batteries. Nature, **414**, 359 (2001). https://doi.org/10.1038/35104644.

[2] Armand M, Tarascon JM. Building better batteries. Nature, **451**,

652 (2008). https://doi.org/10.1038/451652a.
[3] Rahman MA, Wong YC, Song G, Wen C. A review on porous negative electrodes for high performance lithium-ion batteries. J Porous Mater, **22**, 1313 (2015). https://doi.org/10.1007/s10934-015-0010-1.
[4] Etacheri V, Marom R, Elazari R, Salitra G, Aurbach D. Challenges in the development of advanced Li-ion batteries: a review. Energy Environ Sci, **4**, 3243 (2011). https://doi.org/10.1039/c1ee01598b.
[5] Bruce PG, Scrosati B, Tarascon JM. Nanomaterials for rechargeable lithium batteries. Angew Chem Int Ed, **47**, 2930 (2008). https://doi.org/10.1002/anie.200702505.
[6] Aricò AS, Bruce P, Scrosati B, Tarascon JM, van Schalkwijk W. Nanostructured materials for advanced energy conversion and storage devices. Nat Mater, **4**, 366 (2005). https://doi.org/10.1038/nmat1368.
[7] Guo YG, Hu JS, Wan LJ. Nanostructured materials for electrochemical energy conversion and storage devices. Adv Mater, **20**, 2878 (2008). https://doi.org/10.1002/adma.200800627.
[8] Aurbach D, Ein-Eli Y. The study of Li-graphite intercalation processes in several electrolyte systems using in situ X-ray diffraction. J Electrochem Soc, **142**, 1746 (1995). https://doi.org/10.1149/1.2044188.
[9] Nishi Y. Lithium ion secondary batteries: past 10 years and the future. J Power Sources, **100**, 101 (2001). https://doi.org/10.1016/S0378-7753(01)00887-4.
[10] Zhang J, Guo B, Yang Y, Shen W, Wang Y, Zhou X, Wu H, Guo S. Large scale production of nanoporous graphene sheets and their application in lithium ion battery. Carbon, **84**, 469 (2015). https://doi.org/10.1016/j.carbon.2014.12.039.
[11] Vu A, Qian Y, Stein A. Porous electrode materials for lithium-ion batteries: how to prepare them and what makes them special. Adv Energy Mater, **2**, 1056 (2012). https://doi.org/10.1002/aenm.201200320.
[12] Ji L, Lin Z, Alcoutlabi M, Zhang X. Recent developments in nanostructured anode materials for rechargeable lithium-ion batteries. Energy Environ Sci, **4**, 2682 (2011). https://doi.org/10.1039/c0ee00699h.
[13] Zheng F, Yang Y, Chen Q. High lithium anodic performance of highly nitrogen-doped porous carbon prepared from a metal-organic framework. Nat Commun, **5**, 5261 (2014). https://doi.org/10.1038/ncomms6261.
[14] Guo W, Li X, Xu J, Liu HK, Ma J, Dou SX. Growth of highly nitrogen-doped amorphous carbon for lithium-ion battery anode. Electrochim Acta, **188**, 414 (2016). https://doi.org/10.1016/j.electacta.2015.12.045.
[15] Kim NR, Yun YS, Song MY, Hong SJ, Kang M, Leal C, Park YW, Jin HJ. Citrus-peel-derived, nanoporous carbon nanosheets containing redox-active heteroatoms for sodium-ion storage. ACS Appl Mater Interfaces, **8**, 3175 (2016). https://doi.org/10.1021/acsami.5b10657.
[16] Yun YS, Kim DH, Hong SJ, Park MH, Park YW, Kim BH, Jin HJ, Kang K. Microporous carbon nanosheets with redox-active heteroatoms for pseudocapacitive charge storage. Nanoscale, **7**, 15051 (2015). https://doi.org/10.1039/c5nr04231c.
[17] Global forest resources assessment 2015: how are the world's forests changing? Available from: http://www.fao.org/forest-resources-assessment/en/.
[18] Sun X, Wang X, Feng N, Qiao L, Li X, He D. A new carbonaceous material derived from biomass source peels as an improved anode for lithium ion batteries. J Anal Appl Pyrolysis, **100**, 181 (2013). https://doi.org/10.1016/j.jaap.2012.12.016.
[19] Han SW, Jung DW, Jeong JH, Oh ES. Effect of pyrolysis temperature on carbon obtained from green tea biomass for superior lithium ion battery anodes. Chem Eng J, **254**, 597 (2014). https://doi.org/10.1016/j.cej.2014.06.021.
[20] Zhang Y, Zhang F, Li GD, Chen JS. Microporous carbon derived from pinecone hull as anode material for lithium secondary batteries. Mater Lett, **61**, 5209 (2007). https://doi.org/10.1016/j.matlet.2007.04.032.
[21] Selvamani V, Ravikumar R, Suryanarayanan V, Velayutham D, Gopukumar S. Fish scale derived nitrogen doped hierarchical porous carbon: a high rate performing anode for lithium ion cell. Electrochim Acta, **182**, 1 (2015). https://doi.org/10.1016/j.electacta.2015.08.096.
[22] Wang J, Kaskel S. KOH activation of carbon-based materials for energy storage. J Mater Chem, **22**, 23710 (2012). https://doi.org/10.1039/C2JM34066F.
[23] Yun YS, Cho SY, Kim H, Jin HJ, Kang K. Ultra-thin hollow carbon nanospheres for pseudocapacitive sodium-ion storage. ChemElectroChem, **2**, 359 (2015). https://doi.org/10.1002/celc.201402359.
[24] Lian P, Zhu X, Liang S, Li Z, Yang W, Wang H. Large reversible capacity of high quality graphene sheets as an anode material for lithium-ion batteries. Electrochim Acta, **55**, 3909 (2010). https://doi.org/10.1016/j.electacta.2010.02.025.
[25] Yun YS, Park KY, Lee B, Cho SY, Park YU, Hong SJ, Kim BH, Gwon H, kim H, Lee S, Park YW, Jin HJ, Kang K. Sodium-ion storage in pyroprotein-based carbon nanoplates. Adv Mater, **27**, 6914 (2015). https://doi.org/10.1002/adma.201502303.
[26] Ding L, Chen J, Dong B, Xi Y, Shi L, Liu W, Cao L. Organic macromolecule assisted synthesis of ultralong carbon@TiO_2 nanotubes for high performance lithium-ion batteries. Electrochim Acta, **200**, 97 (2016). https://doi.org/10.1016/j.electacta.2016.03.180.
[27] Li X, Geng D, Zhang Y, Meng X, Li R, Sun X. Superior cycle stability of nitrogen-doped graphene nanosheets as anodes for lithium ion batteries. Electrochem Commun, **13**, 822 (2011). https://doi.org/10.1016/j.elecom.2011.05.012.